Journal of Power Sources 302 (2016) 146–154

Contents lists available at ScienceDirect

Journal of Power Sources

journal homepage: www.elsevier.com/locate/jpowsour

Real-time estimation of battery internal temperature based on a simplified thermoelectric model

Cheng Zhang, Kang Li*, Jing Deng

School of Electronics, Electrical Engineering and Computer Science, Queen's University Belfast, 125 Stramillis Road, Ashby Building, Belfast, BT9 5AH, UK

HIGHLIGHTS

- A simplified thermoelectric model of battery thermal and electrical behaviours.
- The interactions between battery thermal and electrical behaviours is captured.
- Real-time battery internal temperature estimation using Kalman Filter method.
- Battery internal temperature estimation RMS error is only about 1°.

ARTICLE INFO

Article history:
Received 6 August 2015
Received in revised form
24 September 2015
Accepted 15 October 2015
Available online xxx

Keywords:
LiFePO4/C battery
Internal temperature estimation
Simplified thermoelectric model
Extended Kalman filter

ABSTRACT

Li-ion batteries have been widely used in the EVs, and the battery thermal management is a key but challenging part of the battery management system. For EV batteries, only the battery surface temperature can be measured in real-time. However, it is the battery internal temperature that directly affects the battery performance, and large temperature difference may exist between surface and internal temperatures, especially in high power demand applications. In this paper, an online battery internal temperature estimation method is proposed based on a novel simplified thermoelectric model. The battery thermal behaviour is first described by a simplified thermal model, and battery electrical behaviour by an electric model. Then, these two models are interrelated to capture the interactions between battery thermal and electrical behaviours, thus offer a comprehensive description of the battery behaviour that is useful for battery management. Finally, based on the developed model, the battery internal temperature is estimated using an extended Kalman filter. The experimental results confirm the efficacy of the proposed method, and it can be used for online internal temperature estimation which is a key indicator for better real-time battery thermal management.

1. Introduction

Due to the imminent challenges of climate change and environment protection, as well as the fast depletion of non-renewable fossil fuels, electric vehicles (EVs) and hybrid electric vehicles (HEVs) are rapidly gaining popularity worldwide in recent years as an effort of replacing the internal combustion engine (ICE) vehicles to improve the fuel efficiency and to reduce the emissions in the transport sector. Lithium-ion batteries are favoured power supplies for EVs and HEVs due to their high power and high energy densities, long service life, high efficiency and environmental-friendly features [1]. A battery management system (BMS) is essential in EV/HEV applications for safe and efficient operation where normally hundreds or even thousands of battery cells are connected in series/parallel configuration to fulfil the high power and high voltage needs of the vehicles [2]. Thermal management is a key part of the BMS, and high temperature is a real threat to safe battery operations. Too high temperature, e.g., over 100 °C, can cause gassing within the battery, electrolyte decomposition, fire or even explosions [2–4]. Even in less severe cases, it has been shown that the lifespan of a Li-ion cell is reduced by about two months for every degree of temperature rise in an operating temperature range of 30–40 °C [5]. Further, although the performance of one battery may heavily rely on its chemistry, choice of material, and cell design, etc., the operation temperature will inevitably affect its electrical performance, such as usable capacity, internal resistance, power ability, and operation safety, etc. For example, according to

* Corresponding author.
E-mail address: k.li@qub.ac.uk (K. Li).

http://dx.doi.org/10.1016/j.jpowsour.2015.10.052
0378-7753/

our experimental studies, the battery usable capacity can drop to less than 80% under 0 °C compared with the nominal capacity under room temperature (25 °C). Under −10 °C, only 65% of the battery nominal capacity is usable. Therefore, proper battery temperature monitoring and management is essential in EV applications.

In practice, only the surface temperature is measurable in real-time for EV battery. Yet, it is the battery internal temperature that directly affects the battery performance, and a large temperature difference may exist between battery internal and surface temperatures (e.g., sometimes greater than 10 °C [6]), especially in high power applications [7]. The battery internal temperature can reach to a critical temperature point a lot quicker than the surface temperature. Therefore, it is insufficient to use the surface temperature measurement alone for battery thermal management. Researchers have proposed in situ battery internal temperature measurement by integrating temperature sensors into the battery internal layers [7,8], but due to additional manufacturing costs and potential safety threat, it has not been adopted in commercialized EV batteries yet. When direct measurement is not available, model based estimation for inferring battery internal temperature offers another option.

Over the years, various battery thermal models of different accuracy and complexity levels have been proposed. Complex distributed electrochemical thermal models for both a single cell and a whole battery pack considering detailed heat generation and dissipation processes within and outside the battery were developed [9–12]. These electrochemical thermal models may be accurate, yet the model complexity is extremely high and usually finite-element method is needed for simulation. Further, many battery chemical and physical parameters involved in these models are difficult to acquire. Simplified lump-parameter thermal models for real-time applications have also been proposed for real-time applications. Smith [13] extracted a 5-node battery thermal model from a detailed Fluent model. Xiao [14] developed a state-space based multi-nodes thermal model using the temperature measurements from various spots on the battery surface.

Lin [15] developed a two-state thermal model and applied for battery internal temperature estimation using an adaptive Kalman filter (KF), where only the heat generation from the battery internal resistance is considered. Sun et al. [16] improved this method by taking into consideration of the heat generation due to entropy change within the battery. Dai [17] adopted the same two-state thermal model and took into consideration of the time-varying model parameters, and applied joint Kalman filter method for the estimation of both the battery internal temperature and the time-varying model parameters. However, none of these papers consider the interactions between the battery thermal and electrical behaviours. The correlation of the thermal and electrical behaviour is however important for battery management. Suppose a constant current is extracted from a battery, and only the heat generation over the battery internal resistance is considered. Then, as the battery temperature increases, the battery internal resistance will drop, which will in turn result in the decrease of overall heat generation. This decreased battery internal resistance will also consequently affect battery electrical performance, such as battery power ability. Therefore, the interaction between battery electric and thermal behaviours should be considered for more accurate battery modelling. It is also noted that due to their correlations, it is possible to infer the battery internal temperature using the battery internal resistance variation information. For example, Hande [18] proposed a method for battery internal temperature estimation by measuring the series battery resistance at cold ambient temperatures.

In summary, to acquire a comprehensive description of the battery behaviours for real-time battery management, the coupling between battery thermal and electric properties should be considered. In the literature, coupled thermal-electrochemical battery models have been developed in Refs. [19,20] using physical laws that govern the battery internal thermal–electrochemical processes. However, these first-principle electrochemical models are not suitable for real-time applications. On the other hand, in the widely adopted simple electric circuit model for battery state-of-charge (SOC) estimation, the temperature effect on battery electric behaviour has been discussed [21,22]. However, as discussed before, most papers only consider the surface temperature, as it is directly measurable.

In this paper, a simplified battery thermoelectric model is built for real-time applications, taking into consideration of the interactions between battery electrical and thermal behaviours. The contributions of this paper are summarized as follows. Firstly, a comprehensive description of battery behaviour is presented by developing a thermoelectric battery model. Secondly, the developed model is used for battery internal temperature estimation, which is a key indicator for better battery thermal monitoring and management. Thirdly, the developed model has a simple structure, and the estimation is based only on the online measured signals, i.e., battery voltage, current and surface temperature measurements. Finally, the proposed Kalman filter method can be implemented in real-time.

The rest of this paper is organized as follows. Section 2 presents the thermoelectric battery model. The test data is described in Section 3. The identified model parameters are given in Section 4, along with the modelling results. Battery internal temperature estimation using Kalman filter method is presented in Section 5, along with the experimental results and analysis. Finally, Section 6 concludes this paper.

2. Battery thermoelectric model

2.1. Battery electric circuit model

There are many different kinds of battery models, such as electrochemical model, reduced order model, electric circuit model and neural networks model, etc [23]. Here we adopt a popular electric circuit model as shown in Fig. 1.where *OCV* is the battery open circuit voltage (OCV), *v*, *i* are the battery terminal voltage and current, respectively. *R* represents the battery internal resistance, and the *RC* network is used to capture the battery relaxation process. Battery OCV is the battery terminal voltage when the battery internal equilibrium is reached in the absence of load. Battery OCV depends on the battery SOC, temperature and previous charging/discharging history, which is referred to as the hysteresis effect. Battery SOC is the charge left in the battery available for further use.

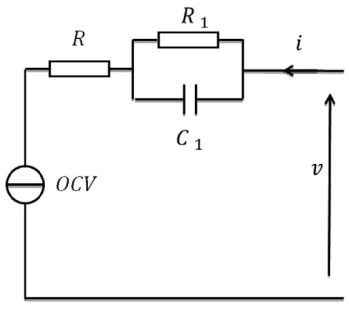

Fig. 1. Battery electric circuit model.

$$soc(k) = soc(k-1) + i(k-1)*T_s/C_n = soc(0) + T_s/C_n* \sum_{j=0}^{j=k-1} i(j) \quad (1)$$

where T_s is the sampling time period in seconds, and C_n is the battery nominal capacity in Ampere second (As), i.e., 1 Ah = 3600 As.

However, according to [24], battery OCV changes slowly with temperature, e.g., less than 10 mV as temperature changes from −10 to 50 °C. Hysteresis effect is also not considered here. The battery voltage after 1-h rest at 25 °C is taken as battery OCV which depends on the battery SOC, as follows,

$$OCV = f_{ocv}(soc) \quad (2)$$

As stated above, battery internal resistance R depends on the battery internal temperature, as follows,

$$R = f_R(T_{in}) \quad (3)$$

where T_{in} is the battery internal temperature. Note that for the LiFePO4/C battery used here, the internal resistance will rise noticeably when the SOC falls below 20%. However, normally EV batteries are only cycled in a limited range, e.g., 30–70% SOC or 20–80% SOC, where the battery internal resistance does not change much with SOC variation.

Suppose the over-potential across the RC network shown in Fig. 1 is v_1, and that the load current keeps constant during the sampling period. Then, following the dynamics of a RC network, we get

$$v_1(k) = a_1*v_1(k-1) + b_1*i(k-1) \quad (4)$$

where $a_1 = \exp(-T_s/R_1/C_1)$ and $b_1 = R_1{}^*(1 - a_1)$.

According to Fig. 1, battery terminal voltage, $v(k)$ can be calculated as,

$$v = OCV + R^*i + v_1 \quad (5)$$

Combining Eqs. (1)–(5), the battery electric model can be described as

$$\begin{aligned} soc(k) &= soc(k-1) + i(k-1)*T_s/C_n \\ v_1(k) &= a_1*v_1(k-1) + b_1*i(k-1) \\ v(k) &= f_{ocv}(soc(k)) + f_R(T_{in}(k))*i(k) + v_1(k) \end{aligned} \quad (6)$$

2.2. Battery thermal model

A battery thermal model consists of two parts: thermal generation and thermal transfer within and outside the battery. There are multi heat generation sources in the battery, such as activation (interfacial kinetics), concentration (species transport) and ohmic losses (Joule heating from movement of charged particles) [3]. Under large load current, battery heat generation is dominated by the ohmic heat generated over battery internal resistance, since this term is proportional to the square of load current. Therefore, in this paper, the battery heat generation is modelled as

$$Q = R^*i^2 \quad (7)$$

Heat transfer within and outside the battery includes heat conduction, convection, and radiation. In this paper, to build a simplified lump thermal model, we assume that battery shell temperature and internal temperature are both uniform, and heat generation is uniformly distributed within the battery. Heat conduction is assumed to be the only heat transfer form between the battery internal and shell, and between the battery shell and the ambience.

The resulting simplified battery model is then given as follows,

$$\begin{aligned} C_1*\frac{dT_{in}}{dt} &= Q - k_1*(T_{in} - T_{sh}) \\ C_2*\frac{dT_{sh}}{dt} &= k_1*(T_{in} - T_{sh}) - k_2*(T_{sh} - T_{amb}) \end{aligned} \quad (8)$$

where T_{in} and T_{sh} are battery internal and shell temperature, respectively; T_{amb} is the ambient temperature; C_1, C_2 are the battery internal and shell thermal capacity, respectively; Q is the generated power in Eq. (7); k_1 is the heat conduction coefficient between the battery internal and the shell, and k_2 the heat conduction coefficient between the battery shell and the ambience. This first order simplified thermal model is widely adopted in battery thermal modelling field [15,17,25].

Let

$$\frac{dT(k)}{dt} = \frac{z-1}{T_s}*T(k)$$

where $zT(k)=T(k+1)$, and discretizing Eq. (8), yields,

$$\begin{aligned} C_1*\frac{z-1}{T_s}*T_{in} &= Q - k_1*(T_{in} - T_{sh}) \\ C_2*\frac{z-1}{T_s}*T_{sh} &= k_1*(T_{in} - T_{sh}) - k_2*(T_{sh} - T_{amb}) \end{aligned} \quad (9)$$

2.3. Coupled thermoelectric model

By combining Eqs. (6), (7) and (9), we get the coupled thermoelectric model as follows,

$$\begin{aligned} x(k+1) &= A^*x(k) + B(k) \\ v(k) &= f_{ocv}(soc(k)) + v_1(k) + f_R(T_{in}(k))*i(k) \\ T_{sh}(k) &= T_{sh}(k) \end{aligned} \quad (10)$$

where

$$x(k) = [soc(k), v_1(k), T_{in}(k), T_{sh}(k)]^T$$

$$A(k) = \begin{bmatrix} 1 & 0 & 0 & 0 \\ 0 & a_1 & 0 & 0 \\ 0 & 0 & 1 - T_s*k_1/C_1 & T_s*k_1/C_1 \\ 0 & 0 & T_s*k_1/C_2 & 1 - T_s*(k_1+k_2)/C_2 \end{bmatrix}$$

$$B(k) = \left[-T_s/C_n*i(k),\ b_1*i(k),\ T_s/C_1*f_R(T_{in}(k))*i^2(k),\ T_s/C_2*k_2*T_{amb}\right]^T$$

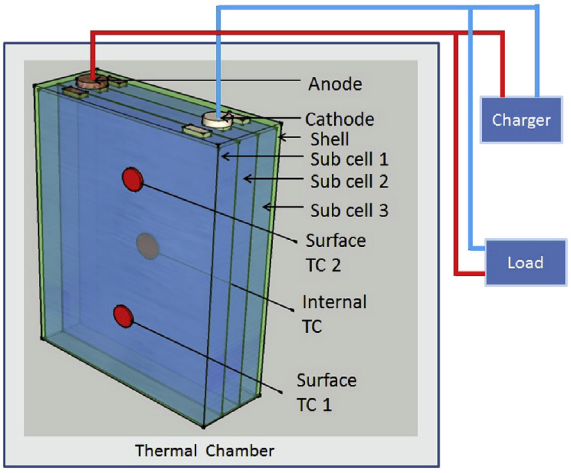

Fig. 2. The battery test system configuration.

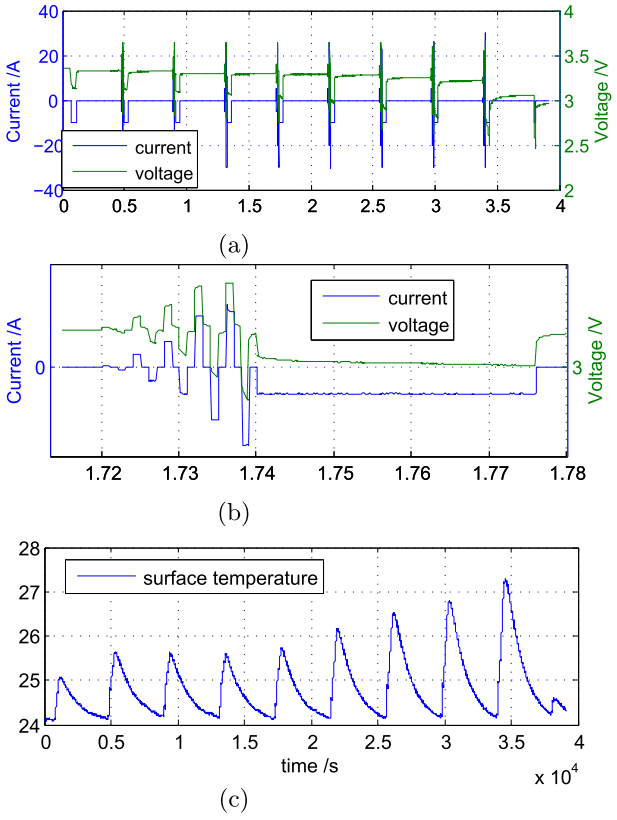

Fig. 3. HPPC discharging test under 23 °C: (a) terminal current and voltage; (b) one zoomed segment of the terminal current and voltage; (c) surface temperature.

As can be seen, the battery internal temperature T_{in} can affect battery electric performance by changing the battery internal resistance R in Eq. (3), while the changing R will in turn affect the heat generation rate in Eq. (7). Unlike the sole battery electric model and sole thermal model, this coupled thermoelectric battery model can capture the interactions between battery thermal and electrical behaviours.

3. Test data

The test system includes a charger, an electric load, and the temperature is controlled by a thermal cabinet, as shown in Fig. 2. The Li-ion battery used in this paper is a prismatic LiFePO4-Graphite battery made by GWL/power Company, and was purchased from the open market. The battery has a capacity of 10 Ah and a nominal operation voltage of 3.2 V. The battery structure includes the outside shell, i.e., the battery can which is made of Aluminium, and the internal layers which can be further divided into three identical sub-cells connected in parallel. Each sub-cell consists of the anode, cathode, electrolyte, current collectors and separators that are wrapped together. Two thermocouples are attached to the battery shell surface, and another thermocouple is inserted into the center area between sub-cell 1 and sub-cell 2. Technically speaking, the battery internal temperature is not measured at the 'cell core area', which usually refers to the core of each individual sub-cell. However, as shown in Fig. 2, this internal temperature measurement is a good indicator of the battery internal temperature.

The battery is firstly fully charged using the standard constant current constant voltage (CCCV) charging method under room temperature (25 °C). Then the battery is put in the thermal cabinet and rests for 1 h. The battery then goes through ten discharging segments, as shown in Fig. 3a for battery terminal voltage current, respectively. Fig. 3b shows one zoomed segment of the voltage and current test data for illustration purpose. Note that the current is positive for charging and negative for discharging. A battery surface temperature measurement is shown in Fig. 3c during this test.

The first segment in Fig. 3a discharges the battery by 1 Ah, i.e., reducing the battery SOC by 10% using 10 A discharging current for 360 s. The following eight segments are the same, as shown in Fig. 3b. The initial several current pulses are used to test battery internal resistance and pulse power ability, followed by 10 A discharging for 360 s to reduce the battery SOC by 10%. The final segment in Fig. 3a fully discharges the battery.

The sampling time period is 1 s, i.e., $T_s = 1$ s.

The above test is repeated under six different temperatures, i.e., [−10, 0, 10, 23, 39, 52] °C.

Besides, two battery self-heating tests are run under 26.3 °C and 5.5 °C ambient temperature. The load current and measured internal and shell temperatures are shown in Fig. 4.

As shown in Fig. 4b and d, under 26.3 °C ambient temperature, battery internal and shell temperature can differ by more than 6 °C, while under 5.5 °C ambient temperature, the temperature difference can be as great as 10 °C. The differences between the two surface temperature measurements are always less than 2 °C, which confirms that the battery shell temperature can be considered as uniform. It is also worth noting that although there exits a temperature difference between different spots on the battery shell, they all follow the same changing dynamics. Further, as can be seen in Fig. 4b and d, $T_{sh}2$ is always lower than $T_{sh}1$. These two figures are so similar that we can reasonably assume that the temperature changing dynamics at each shell spot keep constant in repeated tests, which offers a foundation for estimating battery internal temperature by shell temperature measurement at one spot only.

The designed battery self-heating load current is a continuous 30 A charging-discharging pulse current. However, as can be seen in Fig. 4c, the measured charging current is less than 30 A. This is because that the battery voltage reached a upper voltage limit, i.e., 3.65 V according to the manufacture specification, therefore, the battery charging current is forced to be less than the set value.

It is worth noting is that as shown in Fig. 3c, when this EV

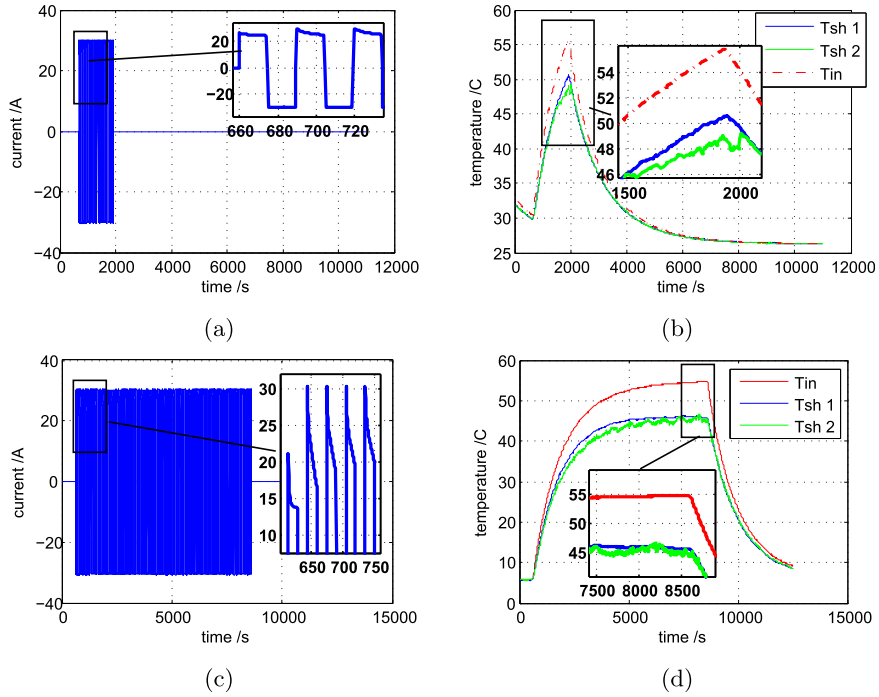

Fig. 4. Battery self-heating test: (a) terminal current under 26.3 °C: (b) temperature measurements under 26.3 °C (c) terminal current under 5.5 °C: (d) temperature measurements under 5.5 °C.

battery was discharged using a 10 A, or 1 C current (for a 10 Ah battery, 1C = 10 A) for 6 min, its shell temperature only increased by about 3 °C. Also as can be seen in Fig. 4d, when the battery shell temperature was 40 °C higher than the ambient temperature, the internal temperature was about 11 °C higher than the shell temperature. Although the temperature gradient between the battery shell and internal may increase if a stronger thermal dissipation is applied, we can still reasonably assume that in low-current applications (e.g., less than 1 C), the battery internal temperature will not differ much from the surface temperature. Therefore, in this paper, we only focus on high load current applications where the battery internal temperature estimation is vital for battery management.

4. Model identification

4.1. Electric model identification

Under laboratory test conditions, battery terminal current and voltage can be accurately measured. Then battery SOC can be calculated by current integration method as in Eq. (1). Since the battery is firstly fully charged at room temperature, therefore battery SOC can be initialized to one, i.e., $soc(0) = 1$ in Eq. (1).

In this paper, we take the battery voltage after 1 h relaxation as the battery OCV. Note that for LiFePO4/C batteries, it normally takes more than 3 h for the battery to finally stabilize. However, according to our test, the voltage difference between 1 h relaxation and 3 h relaxation is less than 5 mV. Also note that after 1 h relaxation, it is reasonable to assume that the battery internal temperature is equivalent to the ambient temperature, as can be seen in Fig. 4b and d. The battery OCV at different SOC level under room temperature is plotted in Fig. 5a.

Battery internal resistance can be calculated by direct calculation method. We know that the time constant of the *RC* network shown in Fig. 1 is larger than 20 s, and sampling period $T_s = 1$. Therefore, when the load current jumps, the instantaneous voltage jump is caused by the series battery internal resistance, i.e., *R* shown in Fig. 1. Therefore, battery internal resistance can be calculated as

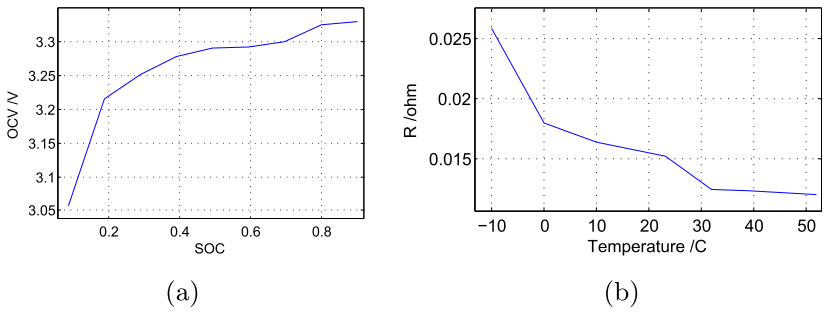

Fig. 5. Battery circuit model elements (a) battery OCV vs SOC under room temperature; (b) battery internal resistance at different T_{in}.

$$R = \frac{v(k+1) - v(k)}{i(k+1) - i(k)},\ when\ \left|i(k+1) - i(k)\right| > I_{th} \tag{11}$$

where I_{th} is a threshold value.

Since the temperature change is a slowly accumulating process, for a short period, the battery temperature can be assumed constant. There are many time points when the load current jumps in one test profile, therefore, a LS fitting is adopted to calculate R. Finally, the calculated R under different temperature is plotted in Fig. 5b.

According to Eq. (5)

$$v_1(k) = v(k) - OCV(soc(k)) - R^*i(k)$$

where $soc(k)$ is calculated by Eq. (1). $OCV(soc(k))$ can be calculated by linear interpolation method based on the recorded data in Fig. 5a. After calculating v_1, Eq. (4) is a standard least square fitting problem.

Let

$$Y_e = [v_1(2), v_1(3), \ldots, v_1(N)]^T$$

, where N is the data length, and

$$\varphi_e(k) = [v_1(k), 1]^T$$

$$P_e = [\varphi_e(1), \varphi_e(2), \ldots, \varphi_e(N-1)]^T$$

, then a_1,b_1 can be calculated as

$$[a_1, b_1]^T = \left(P_e^T * P_e\right)^{-1} * P_e^T * Y_e \tag{12}$$

and modelling error is

$$err = Y_e - P_e * \left(P_e^T * P_e\right)^{-1} * P_e^T * Y_e \tag{13}$$

4.2. Thermal model identification

Based on the measured T_{in}, T_{sh}, and with R calculated by direct calculation method described above, Eq. (9) can also be identified using least square method.

4.3. Modelling results

The identified electric circuit model parameters, i.e., a_1, b_1 under different ambient temperature are very close to each other. Therefore, we adopt a constant RC network to capture the battery relaxation process. The identified electric model parameters are

$$a_1 = 0.982, b_1 = 2.1e-4$$

One segment of the electric modelling results is shown in Fig. 6. The large error spikes in Fig. 6 all occur when the battery load current jumps suddenly. It seems that the simplified battery model cannot capture the fast response after load current changes suddenly. Since the sampling time $T_s = 1$ s, the model cannot capture the battery dynamics in the time scale of less than 1 s. However, the maximum error is less than 50 mV, which is less than 2% of the battery nominal voltage. The root mean square error (RMSE) is about 3.4 mV, which is about 0.1% of the battery nominal voltage. Therefore, the modelling error is acceptable.

The battery self-heating test data under 26.3 °C ambient temperature shown in Fig. 4a are used for battery thermal model parameter identification. The measured shell temperature $T_{sh}1$ is taken as the uniform shell temperature, as shown in Fig. 4b and d. Based on the battery internal temperature measurement, the battery internal resistance R used for calculating the heat generation rate in Eq. (7) can be calculated by linear interpolation method using data recorded in Fig. 5b. The calculated heat generation rate is shown in Fig. 7a. Note that when the battery transits from charging to discharging, the current will go to zero for 1 s, which caused the

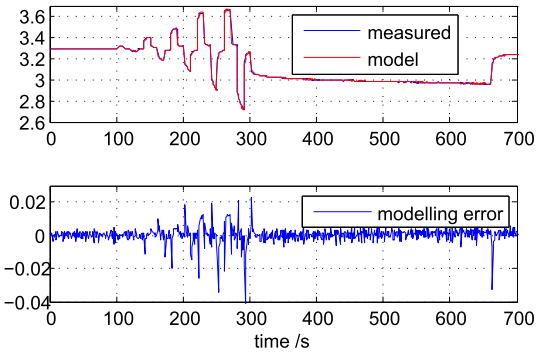

Fig. 6. One part of the electrical circuit model identification results.

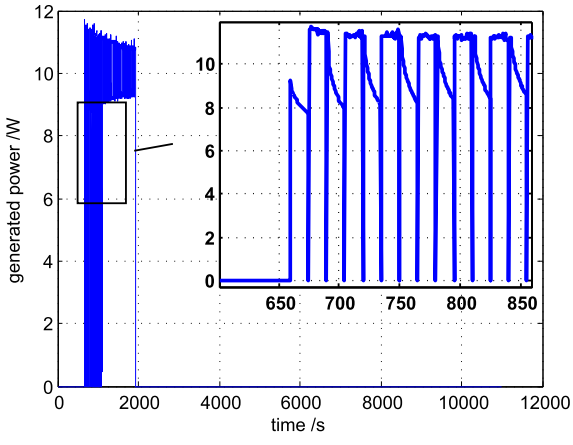

(a)

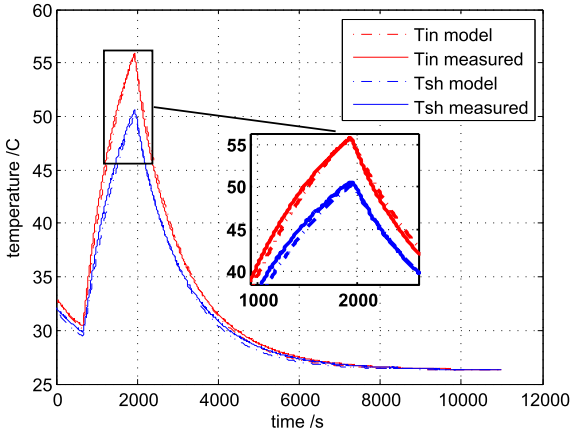

(b)

Fig. 7. Thermal modelling results (a) heat generation rate; (b) thermal model simulation results.

calculated heat generation rate to jump to zero repeatedly in Fig. 7a.

The identified model parameters are,

$$k_1 = 1.286, k_2 = 0.3009$$

$$C_1 = 264.7,\ \ C_2 = 30.7$$

Using the identified thermal model parameters, we run a simulation using Eq. (9). The results are shown in Fig. 7b. The internal temperature modelling RMSE is 0.37 °C, and the maximum error 1.28 °C. The shell temperature modelling RMSE is 0.36 °C, and the maximum error is 1.43 °C.

5. Kalman Filter

After the battery model being identified, it can be used for battery internal states estimation, such as battery SOC and internal temperature T_{in}. Note that in Eq. (10), battery behaviour is described in a state-space formulation. Therefore, various state estimation methods, such as Kalman filter method [26], Unscented Kalman filter method [27] and particle filter method [28], can be used for battery internal state estimation.

Kalman filter has been widely applied for on-line state estimation of linear systems in various applications. Kalman Filter works in a prediction-correction way. The state is firstly predicted using the state equation. Once a new output measurement becomes available, the output prediction error is used to correct the state prediction result. To extend its application to non-linear systems, extended Kalman filter (EKF) is proposed which firstly linearises the system at the current operating point using first-order Taylor series, then Kalman Filter can be applied.

The implementation procedure of EKF is depicted in Table 1.

5.1. KF results

The battery self-heating test data under 5.5 °C shown in Fig. 4 are used for internal temperature estimation. Suppose a 25 °C initial temperature error, and a 15% initial SOC error. The Kalman filter results are shown in Fig. 8.

The Kalman Filter results for temperature estimation are shown in Fig. 8a. As can be seen, it took less than 60 s for the estimated battery internal temperature to converge to the correct one from an initial 25° error. As can be seen, there exits a bias between the estimated T_{in} and the measured T_{in} (about 1 °C from 2000 s to 8000 s in Fig. 8a), which we believe is caused by the inaccuracy of the thermal model. The heat conduction coefficient between battery shell and the ambience should be time-varying [17]. As the ambient temperature drops and battery shell temperature increases, k_2 should increase and more heat be dissipated into the ambience, which will consequently reduce the battery internal temperature. This effect is not considered in this paper. However, the RMSE of T_{in} estimation is 1.01 °C. This estimation result is accurate enough and comparable with the exiting results [25,15,17], which lie between 0.5 and 2 °C.

Apparently, the thermal conductivity coefficient k_2 also depends on the cooling strategy applied to the battery. If a stronger heat dissipation is applied, k_2 will increase. One way to capture this effect is to run tests off-line and identify k_2 under different heat dissipation conditions, and the dependence of k_2 on different heat dissipation methods can be then be tabulated and used in real-time applications. Alternatively, k_2 can be taken as a time-varying model parameters, and a joint-EKF can be applied to estimate both model states and this time-varying parameter simultaneously [17,29]. It is however worth noting that although applying strong heat dissipation will reduce the battery shell temperature, a higher temperature gradient may occur between the battery shell and internal part.

Since the battery shell temperature is directly measurable, the estimated shell temperature matches well with the measured one. Also can be seen in Fig. 8a, the T_{sh} estimation error converged faster than the T_{in} estimation error, which is a reasonable result.

The SOC estimation results are shown in Fig. 8b. As it can be seen, the estimated SOC converged to the correct value from the initial 15% error, and during the self-heating test period (from about

Table 1
Implementation procedure of EKF.

Problem formulation:
State equation:
$x(k+1) = f(x(k),u(k)) + w(k)$
Output equation:
$y(k) = g(x(k),u(k)) + v(k)$
$w(k)$ and $v(k)$ are assumed to be independent Gaussian noise, and
$E(w(k)w^T(k)) = Q(k), E(v(k)v^T(k)) = R(k)$

Calculate:
$A(k) = \frac{\partial f(x,u)}{\partial x}\Big|_{x=\widehat{x}(k)}$
$C(k) = \frac{\partial g(x,u)}{\partial x}\Big|_{x=\widehat{x}_p(k)}$

Initialize
$\widehat{x}(0),\ \ \Sigma(0) = E\{(x(0) - \widehat{x}(0))(x(0) - \widehat{x}(0))^T\}$

For k = 1,2,3, …
1) *Prediction:*
$\widehat{x}_p(k+1) = f(\widehat{x}(k), u(k))$
prediction covariance:
$\Sigma_p(k+1) = A(k)*P(k)*A^T(k) + Q(k)$
2)*Correction:*
Prediction error:
$e(k+1) = y(k+1) - g(\widehat{x}_p(k+1), u(k+1))$
Gain:
$K = \Sigma_p(k+1)*C^T(k+1)*$
$(C(k+1)*\Sigma_p(k+1)*C^T(k+1) + R(k))^{-1}$
Update:
$\widehat{x}(k+1) = \widehat{x}_p(k+1) + K*e(k+1)$
$\Sigma(k+1) = (I - K*C(k+1))*\Sigma_p(k+1)$

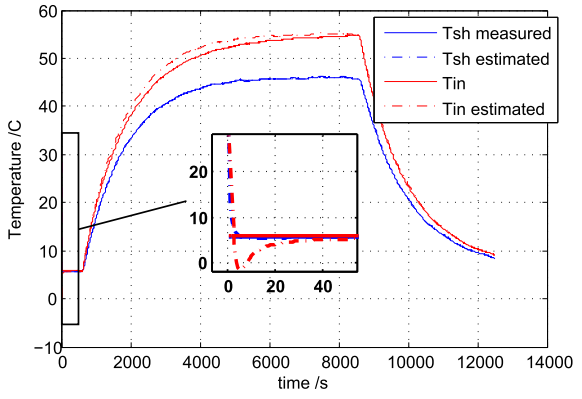

(a)

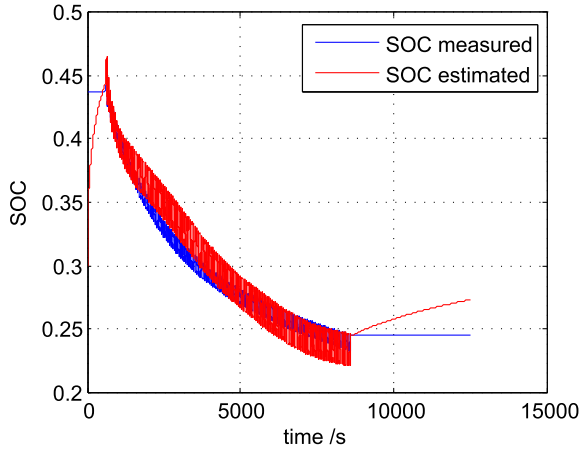

(b)

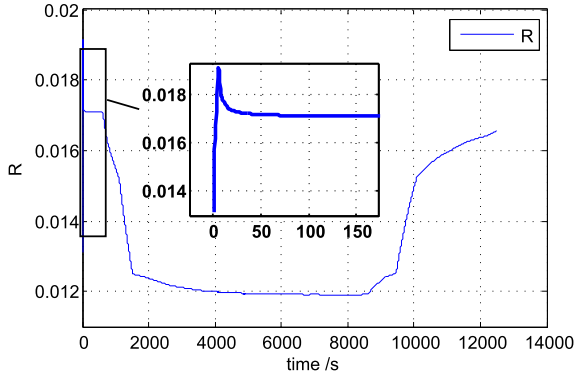

(c)

Fig. 8. KF estimation results (a) temperature estimation; (b) SOC estimation; (c) battery internal resistance estimation.

1000 s to 8000 s in Fig. 8b), the estimated SOC followed the correct SOC curve with good accuracy. During this period, the SOC estimation RMSE is less than 1.5%, which is reasonably good. However, the SOC estimation error increased after the load current is terminated and the battery enters into the relaxation phase. The time constant of the *RC* network adopted in this paper is about 50 s, and its over-potential will fade away in about 200 s. However, the actual relaxation process of the battery will last for hours, as can be seen in Fig. 3a. Therefore, the simplified one RC network model adopted in this paper can not be used to capture the full relaxation dynamics. Also note that the influences of temperature and hysteresis on battery OCV are not considered in this paper. Their effects are of 10 mV level, which is not a big error compared with the 3.2 V nominal battery voltage, therefore it is appropriate for real-time battery thermal management. However, 10 mV can be a large error for accurate SOC estimation, especially for the LiFePO4/C battery used here that has a flat OCV-vs-SOC curve. For better SOC estimation result, a more detailed battery model considering the hysteresis effect and more detailed battery relaxation process should be adopted [30], which is however not the scope of this paper and can be covered in the future research.

The battery internal resistance evolves as battery internal temperature changes, as shown in Fig. 8c. As the battery self-heating process continues and the battery internal temperature increases, the battery internal resistance is reduced. The initial battery internal resistance jump is caused by the wrong initial guess of the battery internal temperature. After the battery internal temperature estimation converged to the correct value, the battery internal resistance converged to the correct value too. Since battery internal resistance significantly affects battery power ability, and sometimes it is used for battery state of health estimation, this real-time estimation of battery internal resistance offers a potential for better prediction of the battery power ability and indicating battery state of health.

Finally, the simplified battery thermoelectric model and internal temperature estimation method developed in this paper can help to develop a proper BMS in EVs. This application can be implemented in multiple ways. Firstly, in terms of off-line applications, this model can be used for simulation of both battery shell and internal temperature responses under different load current profiles and working conditions, which can be used as a guidance for designing thermal management system. For example, this model can be used to calculate the required heat dissipation level (k_2) that can keep the battery internal temperature under a certain level, e.g., 40 °*C* during battery fast-charging operations. Secondly, in terms of online applications, the real-time estimation of the battery internal temperature can serve as a key indicator to help prevent dangerous battery operations that may cause too high temperature inside the battery, especially in high-power demand applications. This can help prolong the battery service life and enhance the safety levels of the battery system, which is currently a major concern in EVs.

6. Conclusion

Battery internal temperature estimation plays a key role in the battery thermal management of electric vehicles for safe and efficient battery operations, especially in high power applications. A novel simplified thermoelectric model is built in this paper considering the interactions between battery terminal electrical behaviour and internal thermal behaviour. Based on this model, battery internal temperature is then estimated using the Kalman filter method in real-time, and serves as an indicator for developing battery thermal management strategies. The proposed estimation method is based only on the online measurable signals, e.g., battery voltage, current and shell temperature, and thus can be implemented in real-time. Test data are collected using a LiFePO4/C battery. The modelling and internal temperature estimation results has confirmed the effectiveness of the proposed method.

Acknowledgement

This research is funded by the EPSRC under the 'Intelligent Grid Interfaced Vehicle Eco-charging (iGIVE)' project EP/L001063/1 and NSFC under the grants 51361130153.

Cheng Zhang would like to thank Chinese Scholarship Council and UK–China Science Bridge project and EPSRC IGIVE project for

sponsoring his research.

References

[1] wikipedia, Electric Vehicle Battery, Feb. 2014. URL, http://en.wikipedia.org/wiki/Electric_vehicle_battery.

[2] L. Lu, X. Han, J. Li, J. Hua, M. Ouyang, A review on the key issues for lithium-ion battery management in electric vehicles, J. Power Sources 226 (2013) 272–288.

[3] T.M. Bandhauer, S. Garimella, T.F. Fuller, A critical review of thermal issues in lithium-ion batteries, J. Electrochem. Soc. 158 (3) (2011) R1–R25.

[4] Z. Rao, S. Wang, A review of power battery thermal energy management, Renew. Sustain. Energy Rev. 15 (9) (2011) 4554–4571.

[5] C.G. Motloch, J.P. Christophersen, J.R. Belt, R.B. Wright, G.L. Hunt, R.A. Sutula, T. Duong, T.J. Tartamella, H.J. Haskins, T.J. Miller, High-power Battery Testing Procedures and Analytical Methodologies for Hev's, Tech. rep., SAE Technical Paper, 2002.

[6] R.R. Richardson, P.T. Ireland, D.A. Howey, Battery internal temperature estimation by combined impedance and surface temperature measurement, J. Power Sources 265 (2014) 254–261.

[7] G. Zhang, L. Cao, S. Ge, C.-Y. Wang, C.E. Shaffer, C.D. Rahn, In Situ Measurement of Temperature Distribution in Cylindrical Li-ion Cells, 226th ECS Meeting, 2014. Cancun, Mexico.

[8] C.-Y. Lee, S.-J. Lee, M.-S. Tang, P.-C. Chen, In situ monitoring of temperature inside lithium-ion batteries by flexible micro temperature sensors, Sensors 11 (10) (2011) 9942–9950.

[9] G.-H. Kim, A. Pesaran, R. Spotnitz, A three-dimensional thermal abuse model for lithium-ion cells, J. Power Sources 170 (2) (2007) 476–489.

[10] Y. Chen, J.W. Evans, Three-dimensional thermal modeling of lithium-polymer batteries under galvanostatic discharge and dynamic power profile, J. Electrochem. Soc. 141 (11) (1994) 2947–2955.

[11] G. Guo, B. Long, B. Cheng, S. Zhou, P. Xu, B. Cao, Three-dimensional thermal finite element modeling of lithium-ion battery in thermal abuse application, J. Power Sources 195 (8) (2010) 2393–2398.

[12] H. Sun, X. Wang, B. Tossan, R. Dixon, Three-dimensional thermal modeling of a lithium-ion battery pack, J. Power Sources 206 (2012) 349–356.

[13] K. Smith, G.-H. Kim, E. Darcy, A. Pesaran, Thermal/electrical modeling for abuse-tolerant design of lithium ion modules, Int. J. Energy Res. 34 (2) (2010) 204–215.

[14] Y. Xiao, B. Fahimi, State-space Based Multi-nodes Thermal Model for Lithium-ion Battery, in: Transportation Electrification Conference and Expo (ITEC), 2014 IEEE, IEEE, 2014, pp. 1–7.

[15] X. Lin, H.E. Perez, J.B. Siegel, A.G. Stefanopoulou, Y. Li, R.D. Anderson, Y. Ding, M.P. Castanier, Online parameterization of lumped thermal dynamics in cylindrical lithium ion batteries for core temperature estimation and health monitoring, Control Syst. Technol. IEEE Trans. 21 (5) (2013) 1745–1755.

[16] J. Sun, G. Wei, L. Pei, R. Lu, K. Song, C. Wu, C. Zhu, Online internal temperature estimation for lithium-ion batteries based on kalman filter, Energies 8 (5) (2015) 4400–4415.

[17] H. Dai, L. Zhu, J. Zhu, X. Wei, Z. Sun, Adaptive kalman filtering based internal temperature estimation with an equivalent electrical network thermal model for hard-cased batteries, J. Power Sources 293 (2015) 351–365.

[18] A. Hande, Internal battery temperature estimation using series battery resistance measurements during cold temperatures, J. Power Sources 158 (2) (2006) 1039–1046.

[19] W. Gu, C. Wang, Thermal-electrochemical modeling of battery systems, J. Electrochem. Soc. 147 (8) (2000) 2910–2922.

[20] V. Srinivasan, C. Wang, Analysis of electrochemical and thermal behavior of li-ion cells, J. Electrochem. Soc. 150 (1) (2003) A98–A106.

[21] M.-H. Chang, H.-P. Huang, S.-W. Chang, A new state of charge estimation method for LiFePO4 battery packs used in robots, Energies 6 (4) (2013) 2007–2030.

[22] F. Baronti, G. Fantechi, L. Fanucci, E. Leonardi, R. Roncella, R. Saletti, S. Saponara, State-of-charge Estimation Enhancing of Lithium Batteries through a Temperature-dependent Cell Model, in: Applied Electronics (AE), 2011 International Conference on, IEEE, 2011, pp. 1–5.

[23] C. Zhang, K. Li, S. Mcloone, Z. Yang, Battery Modelling Methods for Electric Vehicles-a Review, in: Control Conference (ECC), 2014 European, IEEE, 2014, pp. 2673–2678.

[24] LiFePO4 battery temperatures test, URL, http://www.bestgopower.com/technology/documents/temperature-test.html, Jun. 2014.

[25] F. Sun, X. Hu, Y. Zou, S. Li, Adaptive unscented kalman filtering for state of charge estimation of a lithium-ion battery for electric vehicles, Energy 36 (5) (2011) 3531–3540.

[26] R.E. Kalman, A new approach to linear filtering and prediction problems, J. Fluids Eng. 82 (1) (1960) 35–45.

[27] S.J. Julier, J.K. Uhlmann, A new extension of the kalman filter to nonlinear systems, in: Proc. SPIE 3068, Signal Processing, Sensor Fusion, and Target Recognition VI, 1997, pp. 182–193. Orlando, FL.

[28] J. Carpenter, P. Clifford, P. Fearnhead, Improved particle filter for nonlinear problems, IEEE Proc. Radar Sonar Navig. 146 (1) (1999) 2–7.

[29] G.L. Plett, Extended Kalman filtering for battery management systems of lipb-based hev battery packs: part 3. state and parameter estimation, J. Power Sources 134 (2) (2004) 277–292.

[30] C. Zhang, K. Li, L. Pei, C. Zhu, An integrated approach for real-time model-based state-of-charge estimation of lithium-ion batteries, J. Power Sources 283 (2015) 24–36.